NF

NASA CONTRACTOR REPORT 166334

The Influence of Microstructure on the Resistance of Low Strength Ferrous Alloys to Gas Phase Hydrogen Degradation

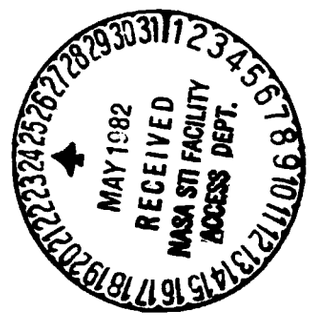

Harry F. Wachob

Failure Analysis Associates

CONTRACT NAS2-9901
May 1981

NASA

NASA CONTRACTOR REPORT 166334

The Influence of Microstructure on the Resistance of Low Strength Ferrous Alloys tc Gas Phase Hydrogen Degradation

Harry F. Wachob
Failure Analysis Associates
750 Welch Road, Suite 116
Palo Alto, California 94304

Prepared for
Ames Research Center
under Contract NAS2-9901

National Aeronautics and
Space Administration

Ames Research Center
Moffett Field, California 94035

ABSTRACT

The role of ferrous microstructure on the near-threshold fatigue behavior has been determined in air and in 6.9 MPa hydrogen. The fatigue crack growth rate at 1 Hertz and $R \tilde{=} 0.15$ was found to be independent of microstructure and strength level for both an A516-G70 and X-60 linepipe steel at alternating stress intensities (ΔK) greater than ~ 15 $MPa \cdot m^{1/2}$. High pressure hydrogen greatly accelerated the fatigue crack growth rate at these ΔK's, but did not alter the observed strength or microstructure independences.

The fatigue threshold values at 10^{-9} ms^{-1} were determined for several normalized, and quenched and tempered microstructures in the A516-G70 steel. For $\Delta K \leq 15$ $MPa \cdot m^{1/2}$ both an austenitic grain size dependence and a strength level dependence of the near-threshold fatigue behavior were observed. The fatigue threshold value increased with increased austenitic grain size and increased yield strength. In addition, the threshold values were found to decrease in a hydrogen environment - the martensitic microstructures showing the largest decrease, normalized microstructures showing the least.

From these results, quenched and tempered microstructures produced at higher austenizing temperatures appear to provide the best static strength and near-threshold fatigue behavior in both air and high pressure hydrogen environments. In conclusion, the ferrous microstructure does influence the near-threshold fatigue behavior in both air and high pressure hydrogen environments.

INTRODUCTION

Growing concern over future energy demands have led to the consideration of hydrogen as a viable energy source, energy storage method, or a transport medium within the United States. Many technological scenarios will store or transport hydrogen at pressures of 7-14 MPa (1000 - 2000 psi). Independent of the methods of production, storage, and distribution, the interaction of hydrogen with its containment material will play an integral role in the success of a hydrogen energy program. Presently hydrogen containment materials can be selected that will remain reasonably free from environmental degradation; however, costly alloying additions are required. High alloy steels are therefore economically prohibitive when large-scale hydrogen storage, transmission, and energy conversion systems are desired. In addition, future critical shortages of major alloying elements used in the production of stainless steel and highly alloyed steels will result in a drastic reduction in the use of these materials in all but the most critical situations. Therefore, to implement such future hydrogen energy systems, existing low-cost materials must be improved via mechanical, thermal, or thermo-mechanical processing or new lost-cost, low-alloy materials which are hydrogen compatible must be developed.

Low strength, low-alloy steels, such as the steels presently used in the natural gas pipeline system, were originally thought to be immune to hydrogen gas embrittlement since no sustained load crack growth had been observed[1]. However, results of Clark[2] in HY80 and Nelson[1] in SAE 1020 showed that the fatigue crack growth rate of these low strength steels can be greatly accelerated by the presence of low pressure hydrogen gas. In recent results

reported by Louthan[3] and Mucci[4], the smooth bar fatigue life of an A106B pipeline steel was reduced by approximately a factor of ten when the tests were performed in a 13.8 MPa hydrogen gas environment. These results suggest that the selection of materials for structures designed to operate in hydrogen under cyclic loads must include a consideration of hydrogen-metal-fatigue interaction.

In addition to laboratory test data, failures of experimental pipeline segments exposed to high pressure hydrogen have been reported[5,6]. Two well documented failures in the Sandia High Pressure Hydrogen Experimental pipeline were attributed to hydrogen accelerated low cycle fatigue.

The fatigue crack growth rate of steels is strongly influenced by service environment, metallurgical condition, and loading parameters. In particular, the near-threshold crack growth behavior of a wide variety of high and low strength steels has been shown to be a function of load ratio (K_{min}/K_{max}), strength level, prior impurity level, and microstructure[7-14]. In particular the behavior of various ferrous microstructures in the slow crack growth rate regime, in a well characterized agressive environment, has not been widely investigated. However in high strength steels, susceptibility to aqueous or internal hydrogen embrittlement has been shown to be sensitive to the metallurgical microstructure[15,16]. In addition, compositional effects and grain size can modify the degree of susceptibility[16]. In general, the best environmental resistance to hydrogen embrittlement seems to be provided by a well tempered martensitic or bainitic microstructure, which has been ausformed to produce refined plate sizes and a finely dispersed array of fine carbides[17,18]; a spheroidized structure of uniformly dispersed carbides is

second best[18,19] with a normalized microstructure being the poorest[18]. This ranking of microstructural resistance to hydrogen degradation has primarily been obtained from aqueous environment tests, which may result in further complications of test interpretation. Unfortunately, a microstructural heirarchy of low or medium strength steels is not presently available for well characterized hydrogen environments.

This research program objective was to determine the role of ferrous microstructure on the near threshold fatigue crack growth behavior of representative pipeline steels. From these results, the least susceptible ferrous microstructure to high pressure hydrogen degradation can be determined. Processing of future pipeline materials to produce this microstructure may then permit a safer and more economical use of our pipeline system. In addition, the microstructure which is most susceptible will also be identified; this may permit the further analysis of critical regions where the local microstructure may be severly degraded, thereby possibly preventing potentially catastrophic failures.

EXPERIMENTAL PROCEDURE

Two steels were used to measure the influence of microstructure on the fatigue crack growth behavior in high pressure hydrogen. Alloy A516-G70 plate was chosen as a steel representative of steels currently used in the natural gas pipeline system. The A516 plate, 1.25 cm thick, was austenitized at either 900°C or 1200°C for 45 minutes, then icewater quenched, isothermally quenched, or furnace fan-cooled. The quenched materials were tempered at 450°C for 1.5 hours. The ambient mechanical properties, corresponding microstructures, and respective processing schedules are listed in Table 1.

TABLE 1

HEAT TREATED PROPERTIES OF A516

CONDITION	YS, MPa	γ-GS, μM	MICROSTRUCTURE
NORMALIZED (AS RECEIVED) 900°C	330	35	PEARLITE-FERRITE
MARTENSITIC γ-900°C IWQ TEMPERED 1.5 hr @ 450°C	905	30	TEMPERED MARTENSITE AND BAINITE
NORMALIZED 1200°C	305	180	PEARLITE-FERRITE
BAINITIC γ-1200°C ISQ - TEMPERED 1.5 hr @ 450°C	415	200	BAINITE WITH CONTINUOUS α-FERRITE AT GRAIN BOUNDARIES (10%)
MARTENSITIC γ-1200°C IWQ TEMPERED 1.5 hr @ 450°C	820	200	TEMPERED MARTENSITE AND BAINITE

A wide range of microstructures and strengths were obtained after the heat treatment of A516. The normalized microstructure is the typical banded pearlite-ferrite commonly seen in hot rolled plate. A representative micrograph of the 70% ferrite - 30% pearlite normalized (900°C) structure is shown in Figure 1. An example of the quench and tempered martensitic structure (1200°C) exhibiting the typical acicular or needlelike martensite platelets is shown in Figure 2. The third microstructure tested is that of an isothermally quenched bainitic or upper pearlitic material. This material has approximately 10% free ferrite in a continuous network at the prior austenite grian boundaries. The overall microstructure and a higher magnification micrograph of a free ferrite region are shown in Figures 3 and 4.

The second steel investigated was a high strength low alloy (X-60 grade) pipeline steel*. This steel is a modern pipeline material whose composition includes low alloy additions for increased strength and improved low temperature toughness. The chemical compositions of both the A516-G70 and the X-60 steels are listed in Table 2. The 1.25 cm base plate contains two submerged arc passes on opposite sides of the plate.(The weld was made parallel to the longitudinal plate rolling directions.) The weld conditions closely approximated those currently employed during linepipe field welding.

There are four distinct microstructural regions associated with the X-60 welded plate. These microstructures - weld or fusion metal, heat affected zone, transition zone, and base metal - are indicated on a macrophotograph of

---

* Dr. John Spingarn of Sandia Laboratory, Livermore, California supplied the material and test specimens for this portion of the program.

Figure 1 - Microstructure of a Normalized A516-G70.

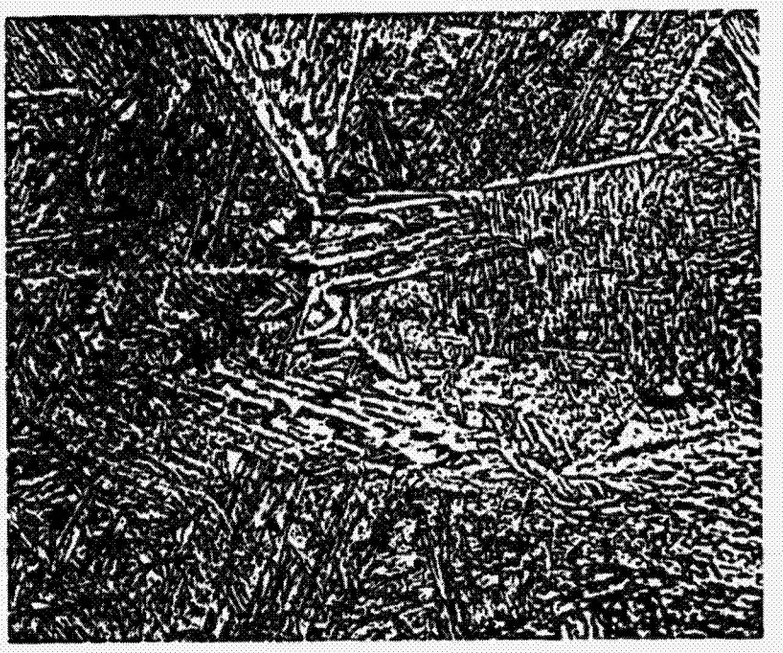

Figure 2 - Quenched and Tempered Martensitic Microstructure Produced After 1200° C Austenitization.

Figure 3 - A516 Bainitic Microstructure.

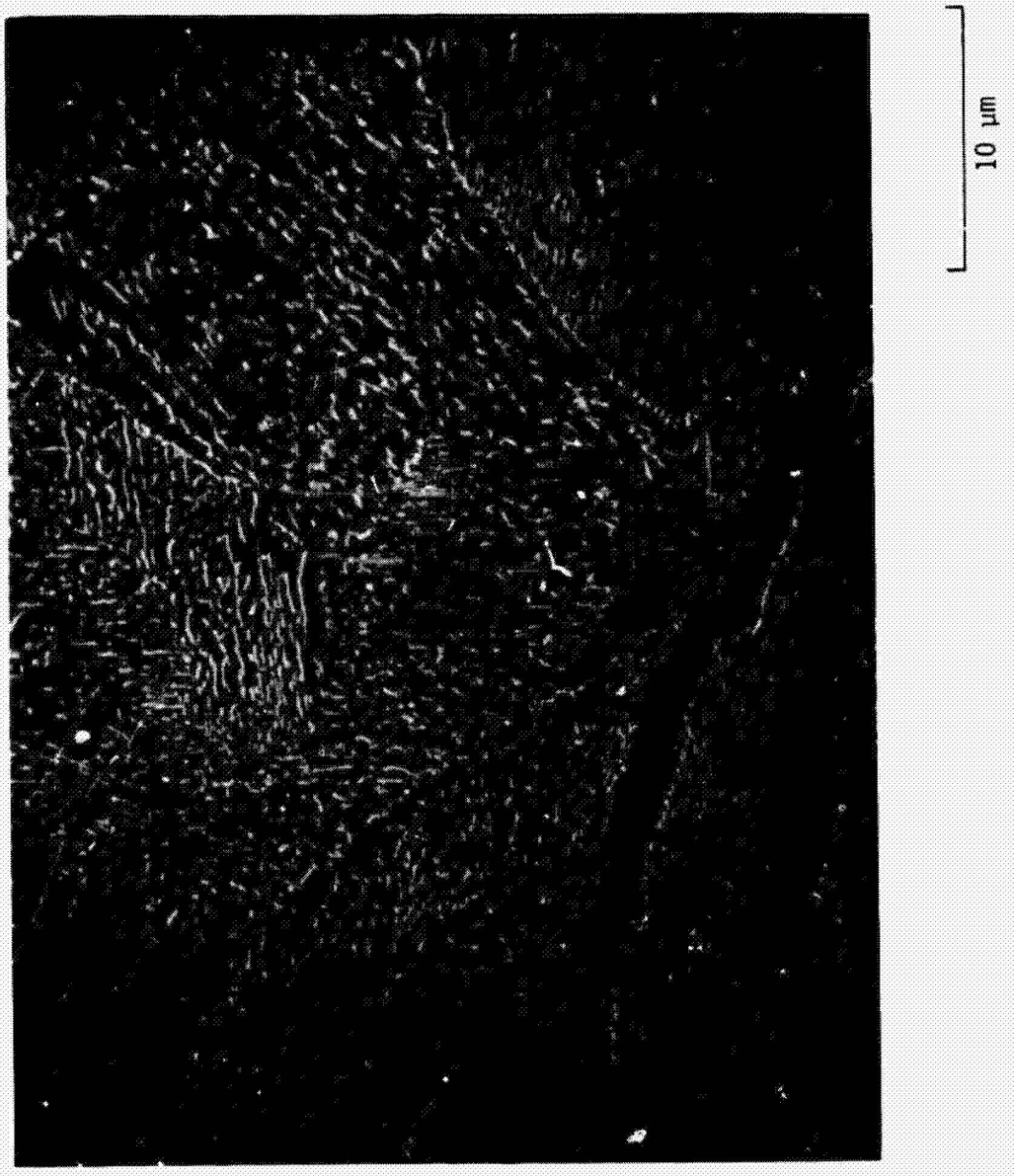

Figure 4 - Carbide Morphology of the Bainitic A516.

TABLE 2

PHYSICAL AND MECHANICAL PROPERTY COMPARISONS
OF A516-G70 AND X-60 LINEPIPE

CHEMISTRY

	C	Mn	P	S	Si	Cu	Ni	Cr	V	Cb	Mo
X-60 Plate	0.12	1.29	.014	.016	.25	.03	.01	.02	.03	.010	.01
A516-G70	0.22	1.10	.009	.023	.21	—	—	—	—	—	—

MECHANICAL PROPERTIES

	σ_Y	σ_{UTS}	ϵ_{TOT}
X-60 Plate	473	675	0.24
A516-G70 (900°C Normalized)	330	565	0.25

the weld in Figure 5. Metallographic examples of each microstructure are also presented in Figure 5. The base plate mechanical properties are given in Table 2 and hardness profiles of the weld region are shown in Figure 6.

TESTING PROCEDURE

Tensile and WOL-compact tension specimens were machined from the heat treated A516 specimen blanks. The tensile axis for the mechanical properties tests were parallel to the long transverse direction while the WOL specimens were in the L-T orientation. The A516 WOL specimens were 1.25 thick and conformed to the ASTM E399-74 standards. For the X-60 material, compact tension specimens of similar geometry were used. In addition the X-60 WOL specimens were taken from the top portion of the plate and were only 0.95 cm thick. The machine notch was carefully placed in either the base metal, the weld metal, or the heat affected zone (HAZ). This variation in notch position permitted the selection and testing of specific microstructures. Since the HAZ was not normal to the base plate surface, the crack front encountered the fusion HAZ, transition zone, and base metal material simultaneously. The effect of the multiple microstructures on the fatigue crack growth behavior will be discussed later.

Tests in high pressure hydrogen were performed in a stainless steel chamber. After the chamber was sealed and evacuated to less than 0.5Pa, it was purged and backfilled slowly with high purity hydrogen. As part of the charging procedure, the hydrogen was passed through a coil submerged in liquid nitrogen to further reduce the water and other possible active gas contaminants. After reading the desired operating pressure of 6.9 MPa, the valve

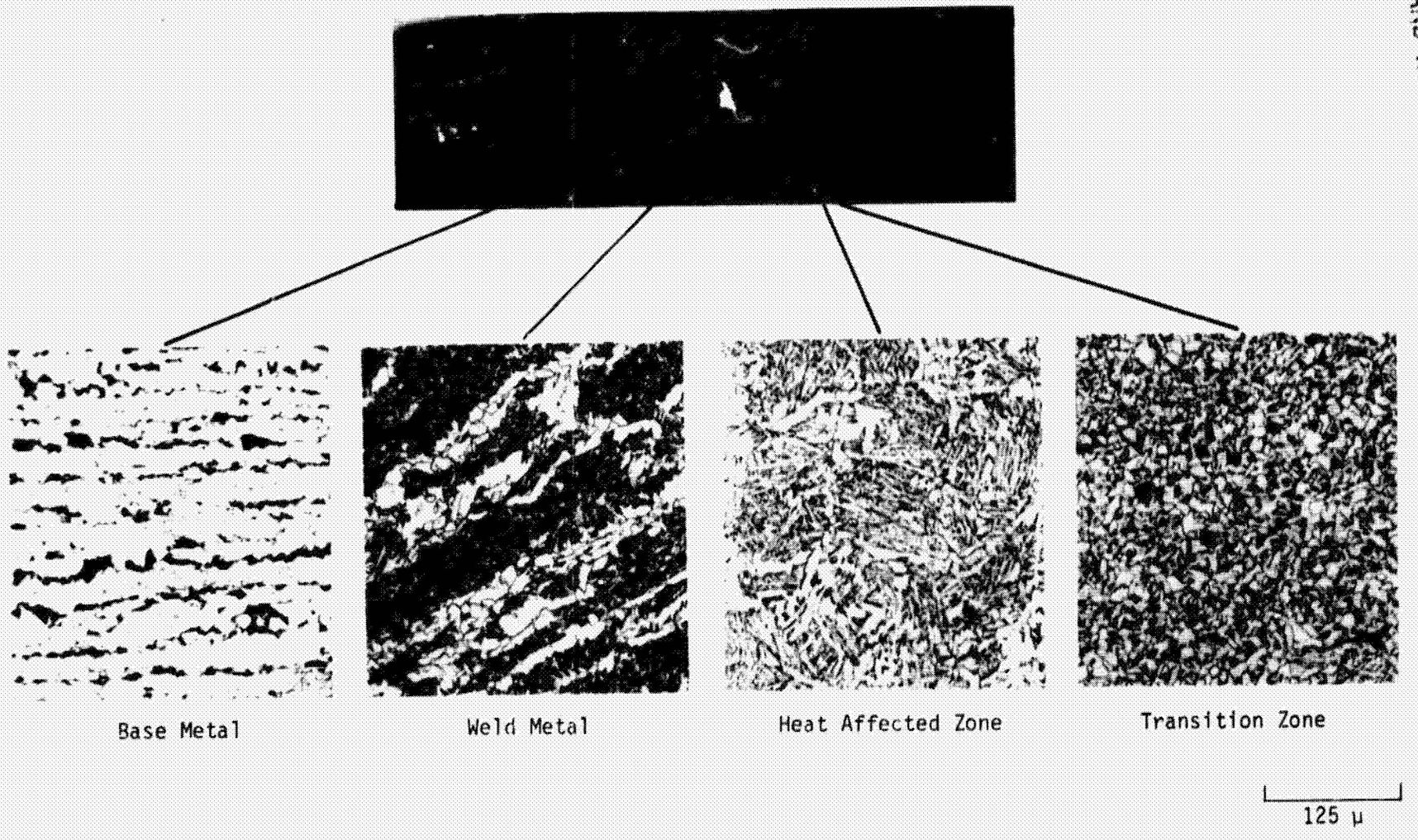

Figure 5 - X-60 Weld Microstructures.

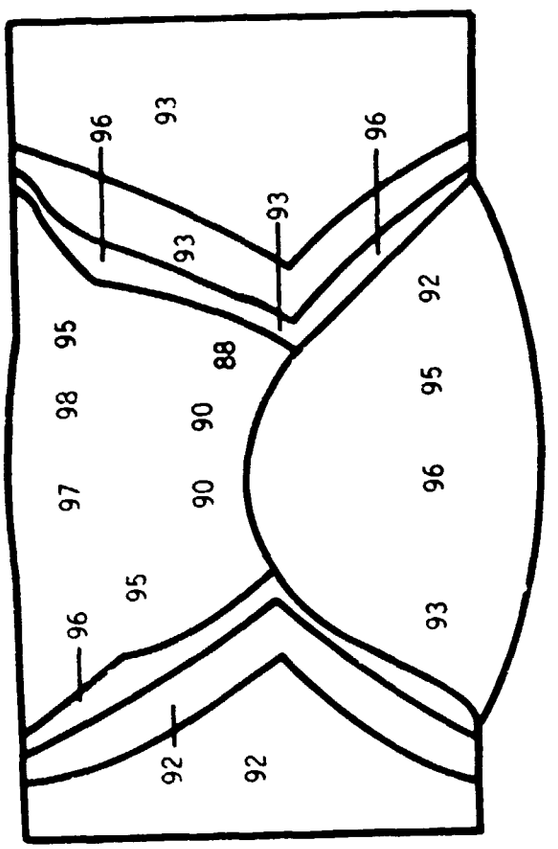

Figure 6 - Rockwell B Hardness for Pipeline Weld.

was closed and the specimen and crack opening displacement gage were allowed to come to equilibrium with the high pressure hydrogen gas for at least 12 hours prior to initiating the test.

The fatigue crack growth rate tests (FCGR) were performed under constant crack opening displacement. This procedure results in an ever decreasing load increment, ΔP (P_{max} - P_{min}), and alternating stress intensity, ΔK, as the crack front extends. The load decay, as a function of cycles, was monitored and later used in the data reduction programs. The stress intensity at the crack tip was calculated using the Newman[19] formulation. This formulation considers the effect of pin loading and applies over a wider range of crack length. The fatigue tests were performed using a 1 Hertz haversine waveform and an R ratio (P_{min}/P_{max}) of ≈ 0.15. The 1 Hz test frequency was a compromise: the 10-80 Hz range which simulates compressor type loading and is commonly used by other experimenters reduces the amount of hydrogen degradation observed; the 1×10^{-4} - 1×10^{-2} Hz range, associated with daily or monthly linepipe pressure fluctuations, requires prohibitively long test periods. The threshold stress intensity was defined as the alternating stress intensity at 10^{-9} m/cycle, the lower limit of experimental resolution.

Fractographic and metallographic analyses were performed after testing was completed. Etching of the metallographic section or fractographic surface was performed using a solution of 4 grams picric acid dissolved in 100 ml of methanol. The surface etching technique frequently permitted the delineation of several microstructural features on the fracture surface.

RESULTS

Tensile Properties of A516

The tensile properties of the various A516 microstructures were determined in air and 6.9 MPa gaseous hydrogen. Hydrogen was found to slightly increase ultimate strength values and to decrease strain to failure. Tests were performed at the plastic strain rates of 2×10^{-2} s^{-1} and 2×10^{-3} s^{-1}. No large strain rate sensitivity was observed, which is in agreement with the results of Banerjee[4]. The reported tensile properties in Table 1 are the average values obtained for that microstructure and strain rates in an air environment. The yield and tensile strengths were not significantly altered by the high pressure H_2 environment. Even though the scatter in the strain to failure and reduction area measurements was large, these parameters were reduced ~ 30% when the tests were conducted in hydrogen. This reduction was probably the result of surface cracking which only occurred during tensile deformation in hydrogen. The extent of the surface cracking was neither uniform from specimen to specimen nor from microstructure to microstructure. The cracking was confined to the necked or post uniform strain regions. These cracks, which were normal to the tensile axis, were of a cleavage or quasi-cleavage nature but were generally only a few grains deep.

Tensile Properties of X-60

Only the base metal mechanical properties were determined for the X-60 material*. A summary of those tests is given in Table 2. However, relative strength levels of individual weld microstructures can be determined from the hardness values (shown in Figure 6).

A516 Fatigue Crack Growth Results

The fatigue crack growth rate (FCGR) of this A516 steel was influenced by a high pressure hydrogen environment and by variations in ferrous microstructure. The FCGR increased and the fatigue threshold value (ΔK_0) decreased in high pressure hydrogen compared with those values obtained in air. In addition, the near-threshold fatigue behavior was strongly influenced by the final austenitizing temperature or austenitic grain size. Details for a given environment and microstructure are presented below.

Baseline fatigue tests were performed in laboratory air (23°C and 45% RH). Fatigue crack growth rates were obtained between 10^{-9} m/cycle and 10^{-6} m/cycle. At $\Delta K \geq 16$ MPa$\cdot m^{1/2}$, the FCGR appeared to be independent of ferrous microstructure or austenitizing temperature, as can be seen in Figure 7. The slope of this linear region in air is 3.8. Below $\Delta K = 16$ MPa$\cdot m^{1/2}$, however, the effect of final austenitizing temperature and strength level on the crack growth behavior becomes apparent. As ΔK decreases, the FCGR decreases rapidly

---

* Mechanical tests performed by Dr. John Spingarn, Sandia Laboratory, Livermore, California.

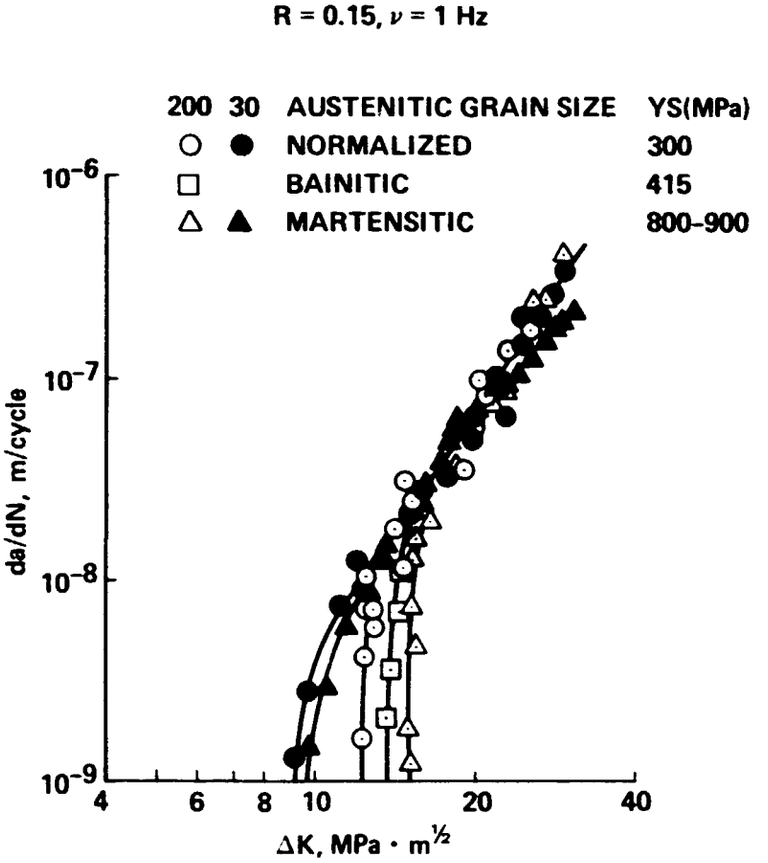

Figure 7 - Fatigue Crack Growth Rate of A516 in Air.

for those specimens austenitized at 1200°C. Threshold values (±1 MPa·$m^{1/2}$) in air were 14 MPa·$m^{1/2}$ for the martensitic structure, 13 MPa·$m^{1/2}$ for the bainitic structure, and 12 MPa·$m^{1/2}$ for the normalized ferrite-pearlitic structure. One important point to note is that the martensitic structure had the highest threshold value--yet had a 50% higher yield strength than the normalized or bainitic structures.

Specimens austenitized at 900°C exhibit a linear crack growth behavior with ΔK above ≈ 11 MPa·$m^{1/2}$ (Fig. 7). Below this limit, the FCGR drops abruptly and approaches threshold values of 9.5 MPa·$m^{1/2}$ for the martensitic structure and 9 MPa·$m^{1/2}$ for the ferritic-pearlitic structure. Again, a slightly higher threshold is obtained in the higher strength martensitic structure.

High pressure hydrogen is found to alter the fatigue behavior of the A516 steel as shown in Fig. 8. For a given ΔK, the FCGR increases above that observed in air when specimens are tested in hydrogen. Also, the fatigue threshold values are lower in hydrogen than in air for all microstructures tested. The general features and shape of the FCGR curves remain similar to the air data as is indicated in Fig. 8.

Above $\Delta K \approx 13$ MPa·$m^{1/2}$ the FCGR in hydrogen appears to be independent of ferrous microstructure and prior austenitic grain size (Fig. 8). The slope of this linear da/dN vs. ΔK curve is about 6.2 which is approximately 60% greater than the slope of 3.8 observed in air. As observed in air, the fatigue thresholds are higher for specimens austenitized at 1200°C than for those austenitized at 900°C. The threshold values for the 1200°C austenitized microstructure are 13 MPa·$m^{1/2}$ for the martensitic structure, 11.5 MPa·$m^{1/2}$ for the

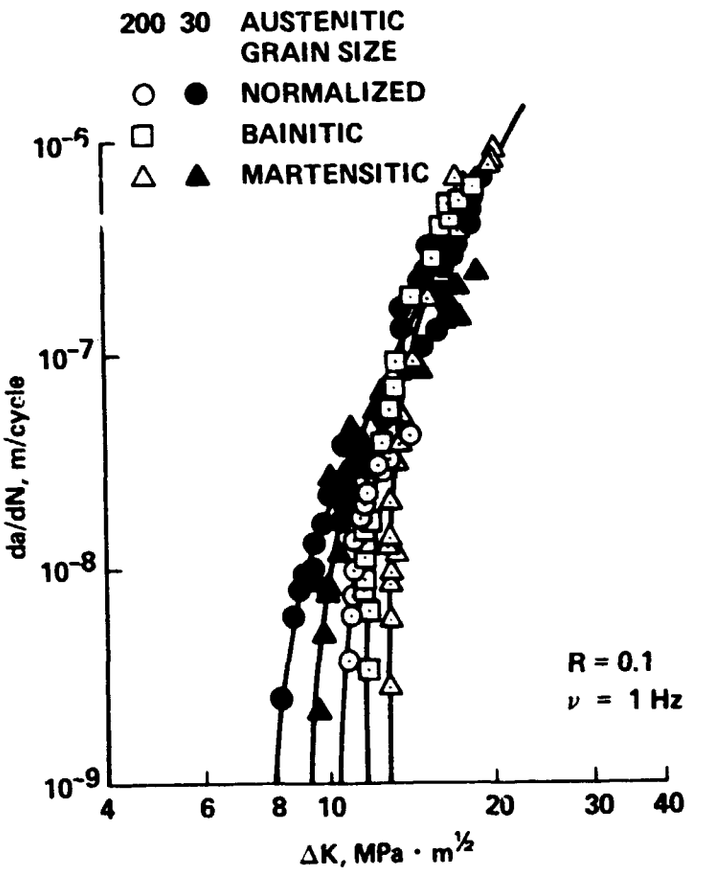

Figure 8 - Fatigue Crack Growth Rate of A516 in 6.9 MPa Hydrogen.

bainitic structure, and 10.5 MPa$\cdot m^{1/2}$ for the ferritic-pearlitic microstructure. The threshold values for the 900°C austenitizing microstructures are 9 MPa$\cdot m^{1/2}$ for the martensitic microstructure and 8 MPa$\cdot m^{1/2}$ for the ferritic-pearlitic microstructure. As had been observed in air, a slight increase in threshold occurs with increased yield strength.

X-60 Fatigue Crack Growth Results

The FCGR of the various X-60 microstructures was similar to that measured for the A516 in both air and high pressure hydrogen. Due to a concern over potential subcritical crack propagation in the microstructures near the HAZ during earlier fracture toughness tests[21], the fatigue crack growth behavior was only measured at ΔK's greater than 10 MPa$\cdot m^{1/2}$. In addition, Ritchie[27] and Mitchell[30] were currently determining the fatigue threshold in X-60 steels at velocities down to 10^{-10} min/cycle. The weld metal, HAZ, and base metal all exhibited similar FCGR's in either the air or hydrogen tests. Under high pressure hydrogen environments, the FCGR of the HAZ specimens tended to fall at the upper bound of the data scatter. However, no statistically significant difference was observed. The air fatigue data appears in Figure 9, with the corresponding hydrogen fatigue results in Figure 10.

A516 Fractographic Results

The effect of hydrogen was to reduce the frequency of fractographic features typically associated with plasticity. The failure mode of the A516 specimens in air was transgranular ductile tearing with evidence of fatigue

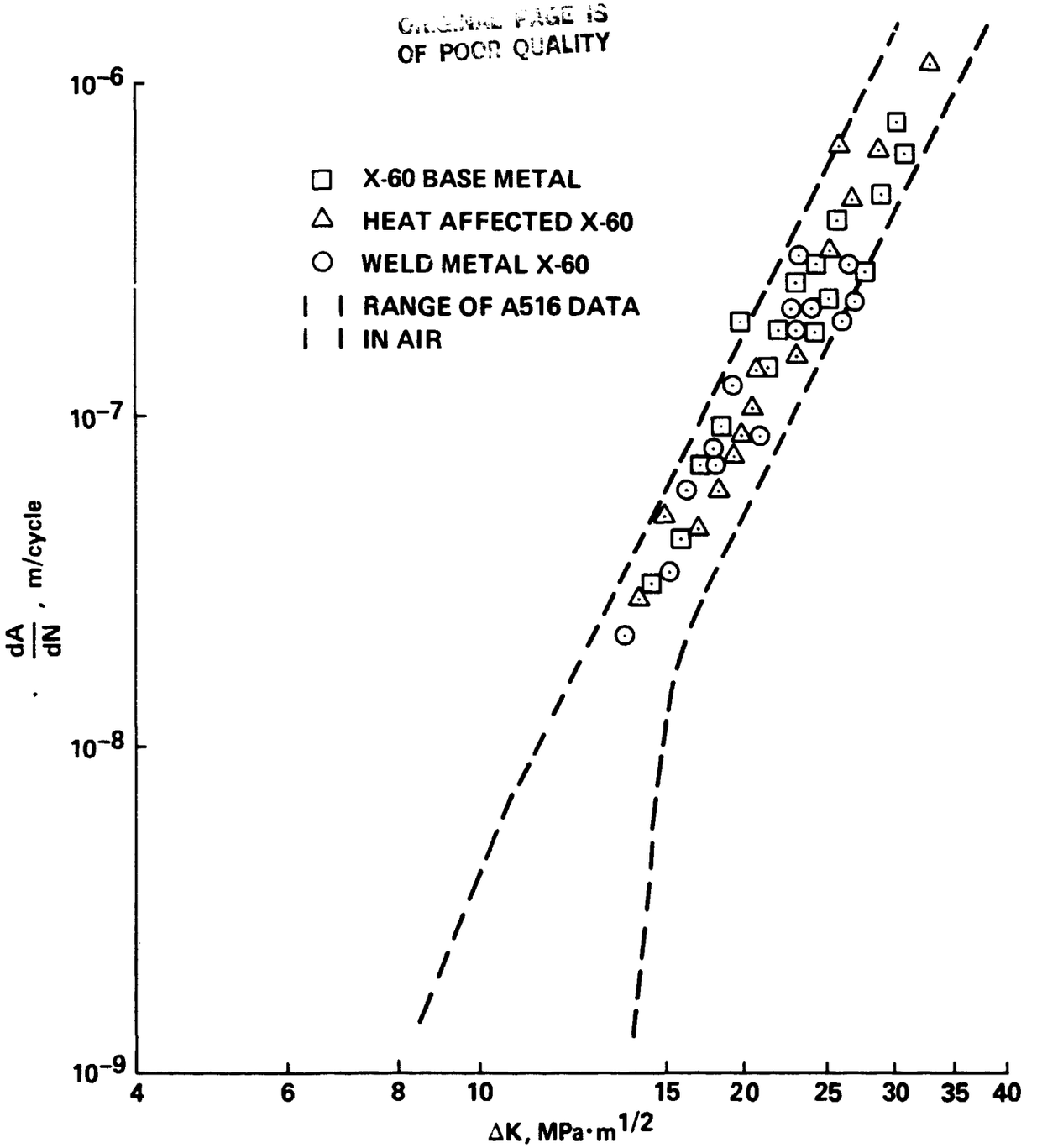

Figure 9 - Fatigue Crack Growth Rate of X-60 in Air.

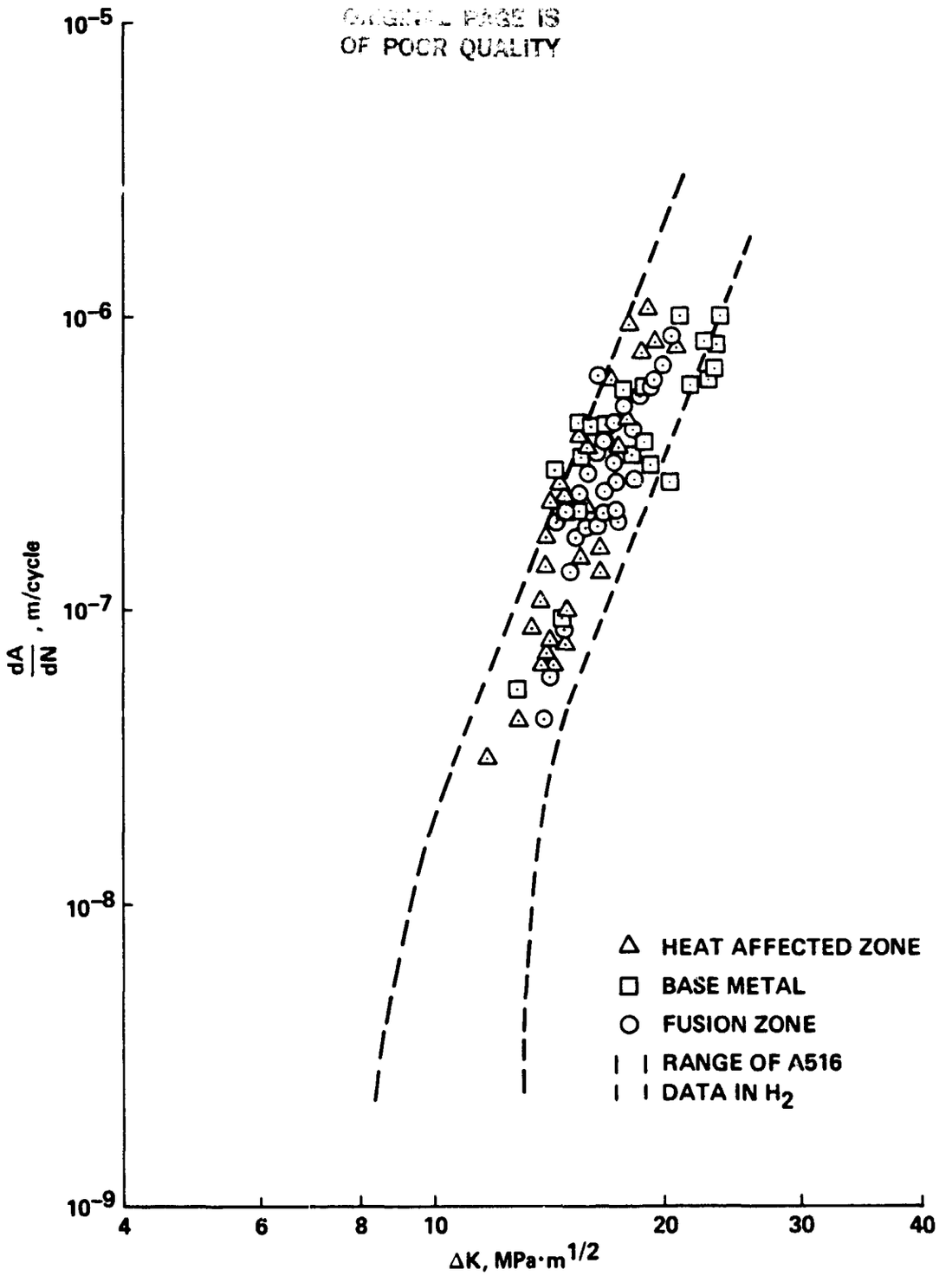

Figure 10 - Fatigue Crack Growth Rate of X-60 in 6.9 MPa H_2.

striations. In hydrogen, the failure mode was either transgranular cleavage or intergranular separation. The ferritic-pearlitic, normalized at 900°C, the martensitic austenitized at 1200°C, and the bainitic isothermally quenched from 1200°C exhibit all of the various fractographic features and therefore will be used to illustrate the individual characteristics.

The crack growth morphology of the normalized microstructure changed drastically upon going from ambient conditions to a high pressure hydrogen environment. A general summary of the primary fractographic features is given in Table 3. The major features observed after air fatigue of the 900°C normalized microstructure are:

1. Fatigue striations and ductile tearing of the α-ferrite, as shown in Figure 11, are the result of plastic blunting and resharpening of the crack tip.

2. Strong influence of the rolling inclusions of MnS, appeared as sharp elongated secondary cracks on the fracture surface, as indicated by the arrows in Figure 12.

3. Frequent secondary cracks along the pearlite-α-ferrite interface, as is shown in Figure 13.

These features were seen over the entire range of alternating stress intensity. However, as the alternating stress intensity, ΔK, decreased, there were indications of less overall gross plasticity associated with the fracture process.

TABLE 3

FRACTOGRAPHY OF NORMALIZED A516

ENVIRONMENT	ΔK, MPa · $m^{1/2}$ RANGE	FEATURES
AIR	10-30	–DUCTILE TEARING, FATIGUE STRIATIONS
		–STRONG INFLUENCE OF MnS
		–LARGE AMOUNT OF SECONDARY CRACKING AT PEARLITE-FERRITE
H_2	~24	–TRANSGRANULAR
		–REDUCED MnS EFFECT
		–DECREASED FREQUENCY OF SECONDARY CRACKS
	~17	–TRANSGRANULAR THRU α - FERRITE
		–SMALL AMOUNT INTERGRANULAR
		–EVIDENCE OF PLASTIC DEFORMATION
	~12	–INTERGRANULAR AT BOTH $\alpha - \alpha$ AND α - PEARLITE BOUNDARIES
		–SMALL AMOUNT TRANSGRANULAR

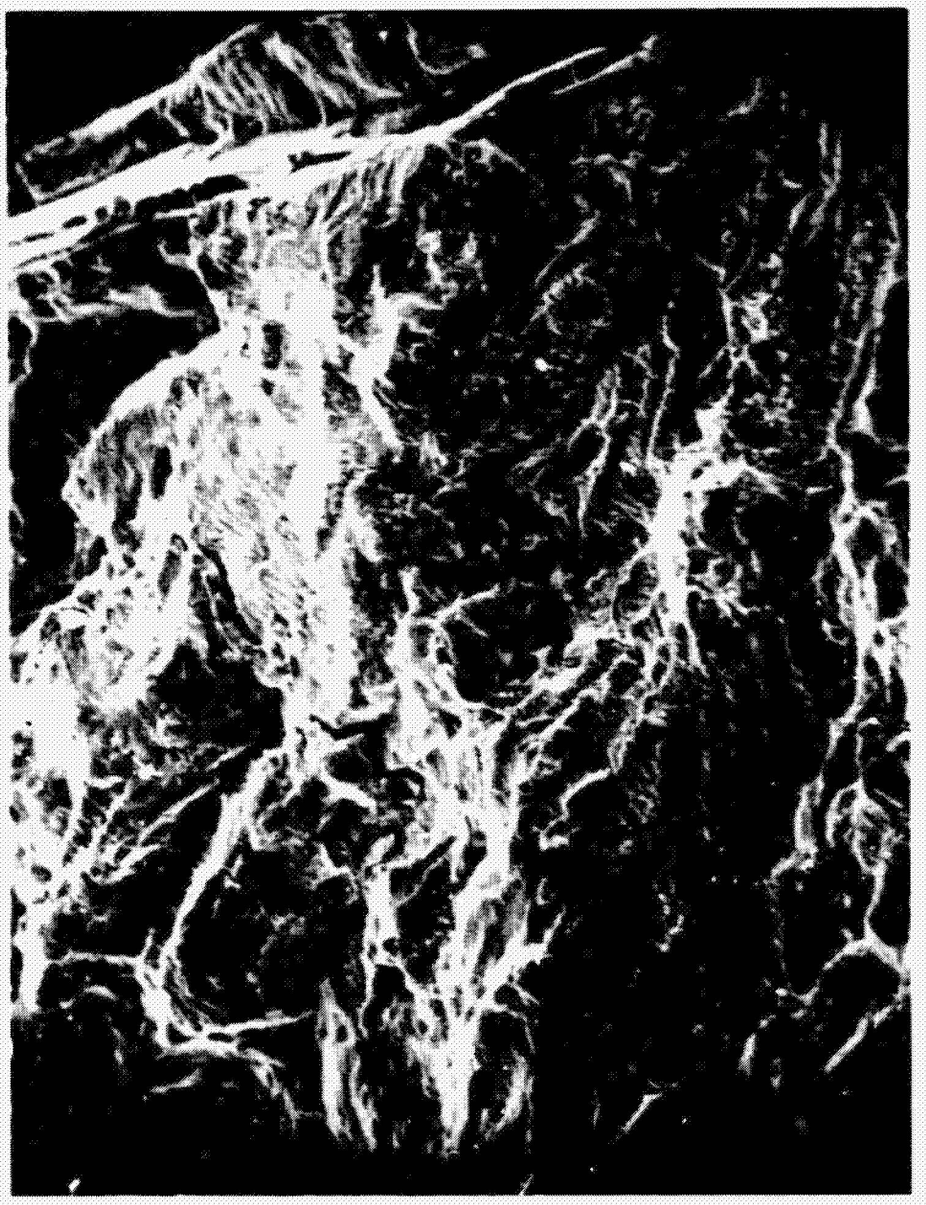

Figure 11 - Typical Air Fatigue Fracture Surface.

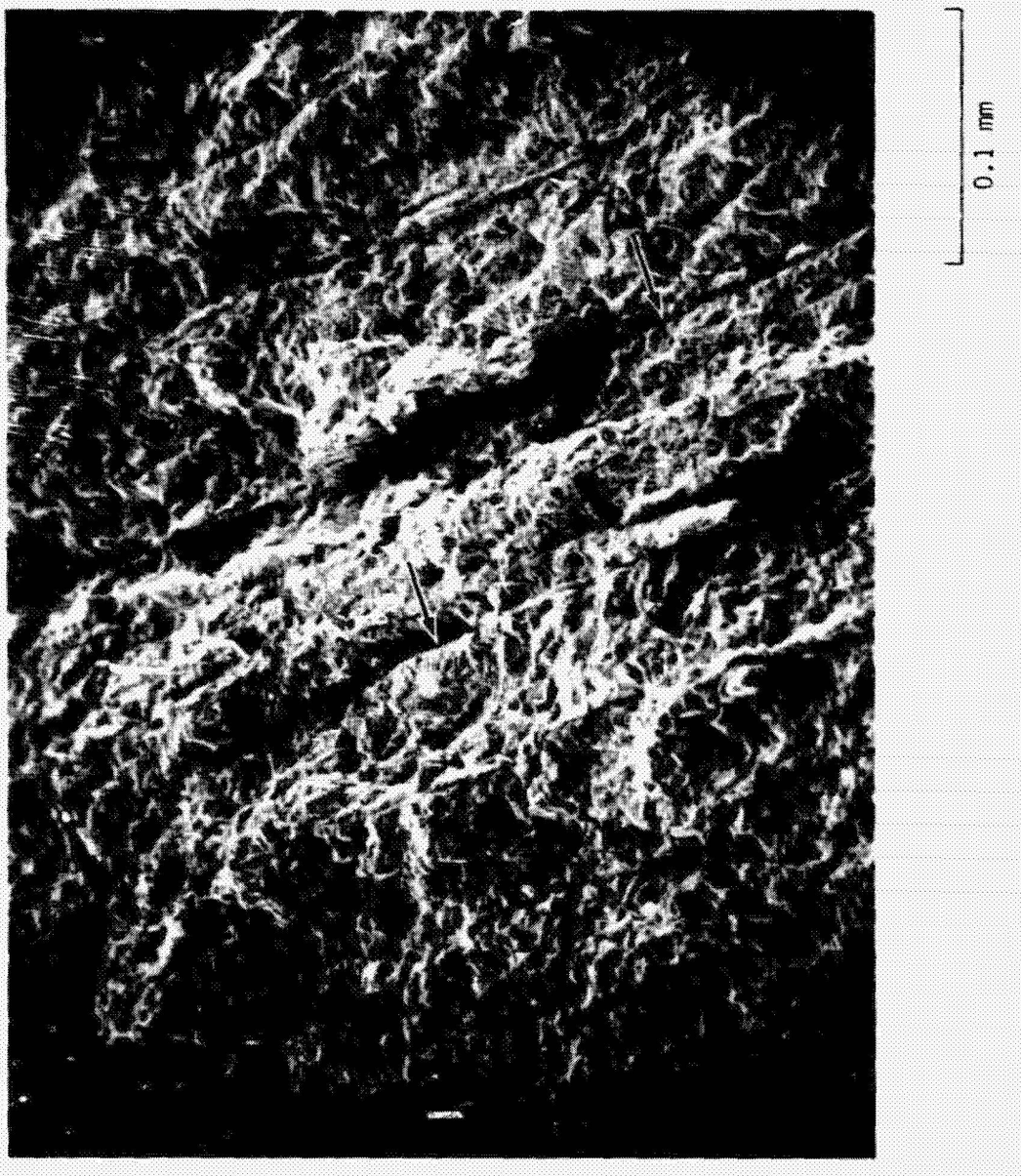

Figure 12 - MnS Domination of Fatigue Fracture.

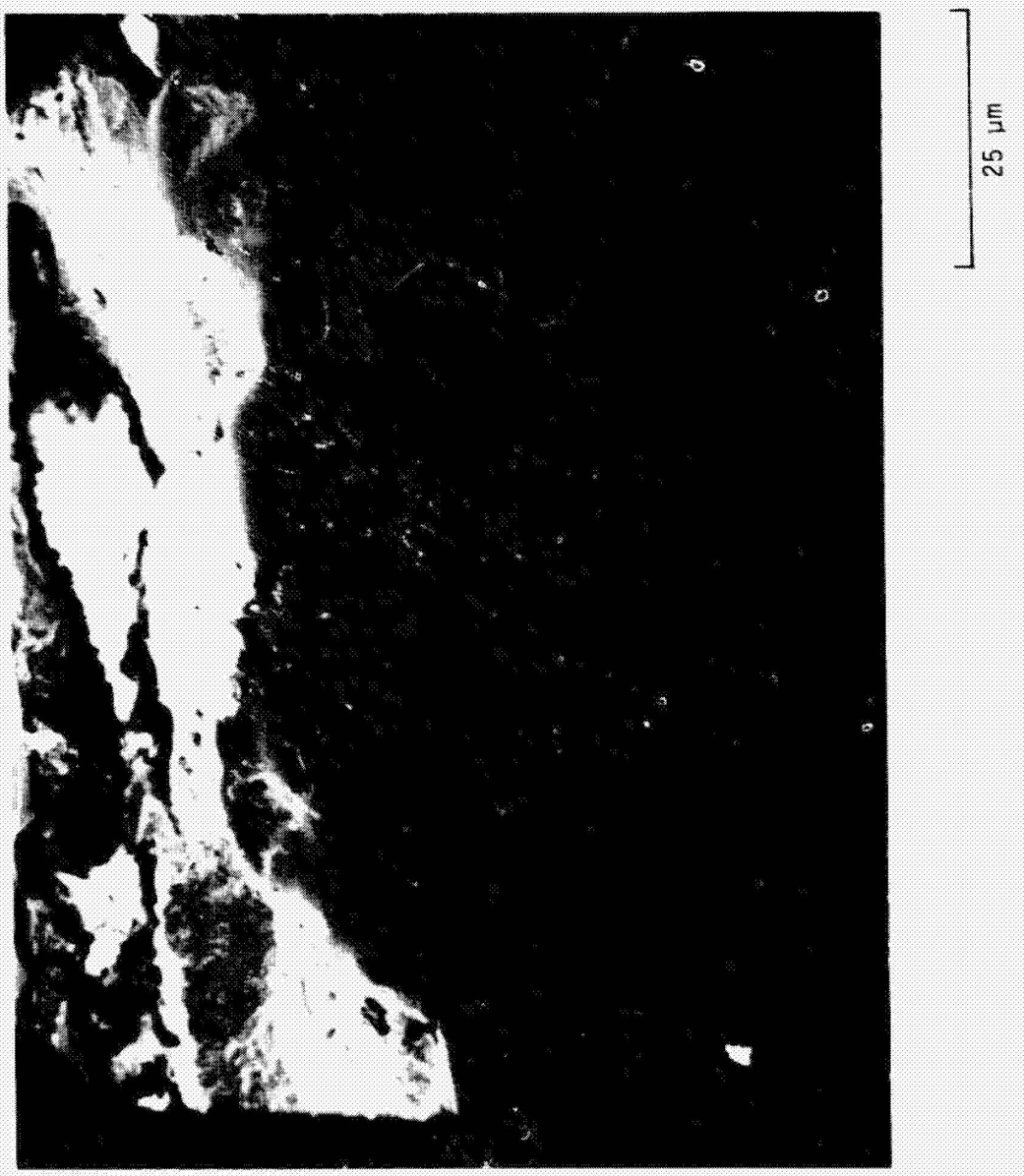

Figure 13 - Secondary Fatigue Cracks Produced in Air.

When the 900°C normalized specimens were fatigued in 6.5 MPa hydrogen, the following fractographic features were observed at various levels of ΔK:

1. At $\Delta K \sim 24$ MPa$\cdot m^{1/2}$, a transgranular mode of failure through both pearlite and ferritic grains occurred, an example of which is shown in Figure 14. In addition to the transgranular failure, evidence of secondary cracking and MnS inclusion effects were absent.

2. At a slightly lower ΔK, ~ 17 MPa$\cdot m^{1/2}$, small amounts of intergranular failure were observed among the general transgranular features. These features were accompanied by a the reduction in the overall amount of ductile tearing.

3. Finally, at ΔK values < 12 MPa$\cdot m^{1/2}$, the fracture surface was primarily intergranular in nature. These intergranular failures occurred at both ferrite-ferrite and ferrite-pearlite boundaries. Figure 15 and 16 illustrate the general appearance of the intergranular failure at low and high magnifications respectively.

The interesting observation is that although the fracture morphology differs greatly for the two environments, the threshold values at 10^{-9} m/cycle are approximately the same.

Figure 14 - Transgranular Fracture of A516 in 6.9 MPa H_2.
$\Delta K \simeq 24$ MPa $\cdot$ $m^{\frac{1}{2}}$

Figure 15 - Intergranular Failure of A516 in 6.9 MPa H_2.
$\Delta K \simeq 12$ MPa $\cdot$ $m^{\frac{1}{2}}$

Figure 16 - Interface of Pearlite - Ferrite Facet.

Hydrogen reduces the occurrence of features typically associated with plastic deformation for the quenched and tempered microstructures. The failure mode of both the 1200°C bainitic and 1200°C martensitic microstructures was primarily a transgranular failure in both hydrogen and air environments. The general fractographic features have been summarized in Tables 4 and 5, respectively.

Bainitic failure surfaces produced in air show some evidence of plastic tearing, transgranular failure, and small amounts of intergranular separation at ferrite-pearlite boundaries. Several of these features and the reduction of secondary cracking at MnS inclusion sites, indicated by arrows, are shown in Figure 17. Only the microstructures austenitized at 1200°C showed evidence of globular or cylindrical MnS inclusions. Those specimens treated at 900°C had large platelet MnS inclusions which acted as secondary crack initiation sites. There are some indications that the crack front in the bainitic specimens followed the lathe interface which resulted in the herringbone appearance in Figure 18. The failure surface also contains an intergranular component. This mode of failure, independent of environment, always occurs at the ferritic-pearlitic boundaries a example of which is shown in Figure 19. This interface was the result of the isothermal tempering. This resultant microstructure is a combination of upper bainite, fine pearlite, and free ferrite at the prior austenite grain boundaries, as was seen earlier in Figures 3 and 4.

The fractographic features of the bainitic fatigue surfaces produced in high pressure hydrogen show less evidence of plastic deformation than observed in air; some intergranular failure and occasional areas of quasi-cleavage of

TABLE 4

FRACTOGRAPHY OF BAINITIC A516

ENVIRONMENT	ΔK, MPa · $m^{1/2}$ RANGE	FEATURES
AIR	15-30	– HERRINGBONE TRANSGRANULAR FAILURE – REDUCED MnS EFFECT – SOME INTERGRANULAR FAILURE AT PEARLITE-α-FERRITE BOUNDARIES – STEPPED CRACK FRONT
H_2 (6.9 MPa)	11-20	– TRANSGRANULAR FAILURE – INTERGRANULAR AT PEARLITE- α-FERRITE – QUASI- CLEAVAGE IN G.B. FERRITE

TABLE 5

FRACTOGRAPHY OF QUENCH AND TEMPERED A516

ENVIRONMENT	ΔK, MPa · $m^{1/2}$ RANGE	FEATURES
AIR	15-30	– TRANSGRANULAR FATIGUE STRIATIONS – SMALL AMOUNTS OF INTERGRANULAR FAILURE
H_2 (6.9 MPa)	13-20	– TRANSGRANULAR CLEAVAGE – REDUCED PLASTICITY – 10% INTERGRANULAR FAILURE

Figure 17 - Fractography of Bainitic Specimen After Air Fatigue.

Figure 18 - Herringbone Transgranular Failure of Bainitic Specimen After Air Fatigue.

Figure 19 - Intergranular Failure of a Bainitic Specimen After Air Fatigue.

the grain boundary ferrite were also observed. These features are illustrated in low and high magnification fractographs in Figure 20 and 21. Again, the fracture path is dominated by the bainitic lathe and grain boundary ferrite.

Martensitic fractographic features are similar to those observed on the bainitic failure surface. The fracture path in air, shown in Figure 22, is crystallographic in nature due to the martensitic packet morphology. At higher magnification, see Figure 23, plasticity and the strong influence of the martensitic microstructure on the failure surface can be seen. In the hydrogen environment, the transgranular failures exhibit less plasticity, as is illustrated by Figure 24 and 25. Additionally, the amount of intergranular failure increases to approximately 10%.

X-60 Fractographic Results

As with the A516 microstructures, hydrogen decreases the amount of plasticity typically associated with comparable air fatigue surfaces. Hydrogen environment tests result in flatter fracture surfaces, as compared to the more torturous, 3-D surfaces produced during fatigue in air. However, in contrast to the A516 material, several similar fractographic features appear on both the hydrogen and air fatigue surfaces for all the X-60 microstructures investigated. Qualitatively the fracture surfaces are composed of flat transgranular regions surrounded by varying amounts of plastic tearing or local ductile overloads. The ratio of percent transgranular to percent ductile failure increases in the high pressure hydrogen environment.

Figure 20 - Fractography of Bainitic Specimen After Fatigue in 6.9 MPa H_2.

Figure 21 - Transgranular Failure in a Bainitic Specimen After Fatigue in 6.9 MPa H_2.

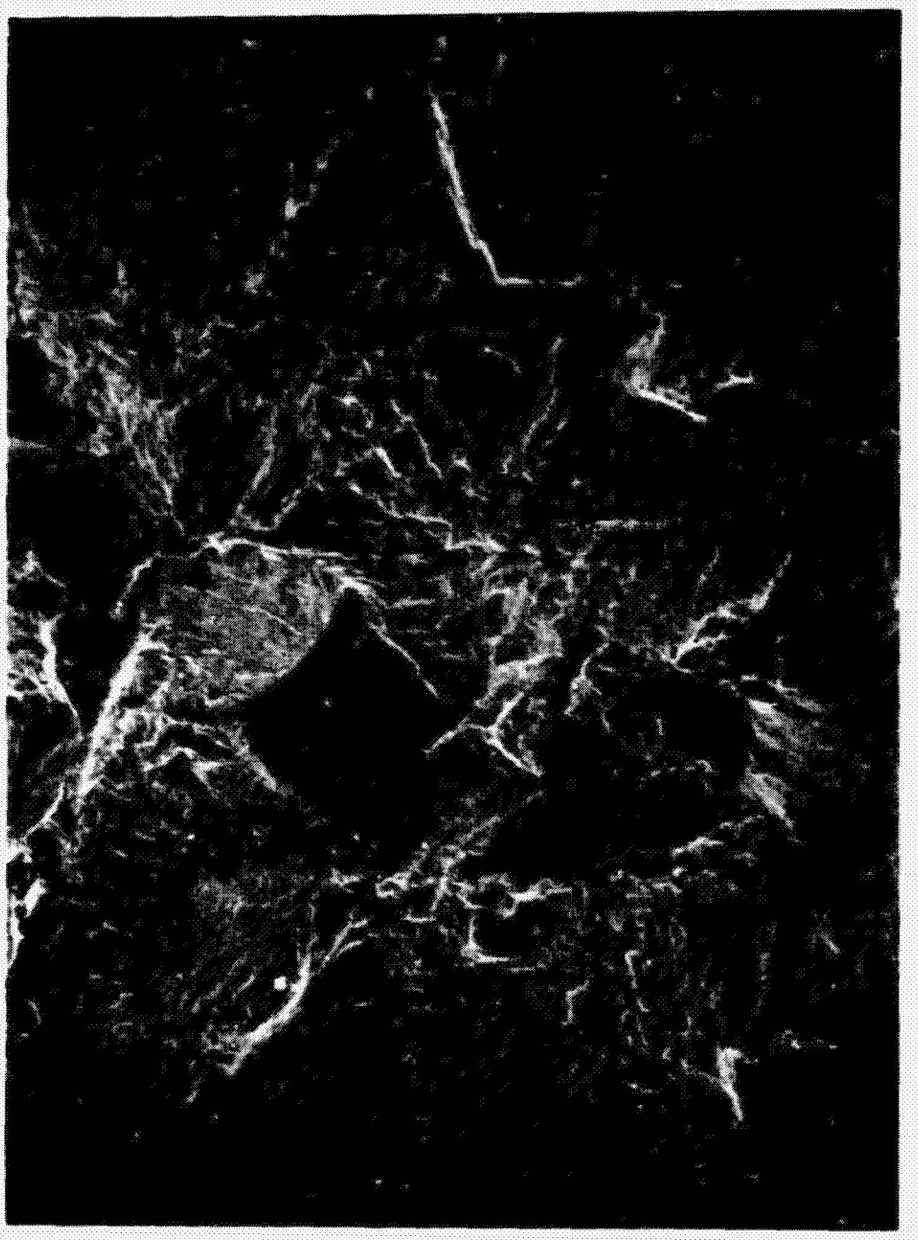

Figure 22 - Typical Fracture Surface of a Martensitic Specimen After Fatigue in Air.

Figure 23 - Transgranular Failure Surface of a Martensitic Specimen After Fatigue in Air.

ORIGINAL PAGE
BLACK AND WHITE PHOTOGRAPH

Figure 24 - Typical Martensitic Fracture Surface Produced by Fatigue in 6.9 MPa H_2.

Figure 25 - Transgranular Packet Fracture of a Martensitic Specimen Fatigued in 6.9 MPa H_2.

Several fractographic features observed for particular microstructures deserve further discussion. One such feature not observed in the normalized A516 microstructures tested in hydrogen is the coexistence of cleavage and cyclic-transgranular flat fracture of the ferrite grains in the same region. Such areas exist in both the weld and base metals. These are illustrated in a low magnification area Figure 26a and more detailed fractographs in Figures 26b and 26c. Small amounts of intergranular failure were also observed in these two microstructures in both environments. The incidence of secondary, intergranular cracking increased sharply when the base metal was tested in high pressure hydrogen environments. An example of this cracking mode is shown in Figure 27.

Discussion

The influence of microstructure on the fatigue behavior of A516 steel in air parallels previous observations for a wide variety of plain carbon steels. The FCGR in air at high ΔK values (> 15 MPa$\cdot m^{1/2}$) is in good agreement with the literature results of SAE 1020[2], A516-G60[22], A516-G70[23], and several specially prepared Fe-C alloys[24,25]. This agreement of FCGR's suggests that for the low-alloy, low-strength steels, compositional and minor strength differences do not affect the air crack growth rates substantially. In addition, the present results for the X-60 base metal and various welded microstructures are also in good agreement with these reported FCGR's. This agreement suggests that the minor alloy additions of Ni, Cr, V, Nb, and Mo do not affect the general fatigue behavior even though they increase the strength and improve the low temperature fracture toughness.

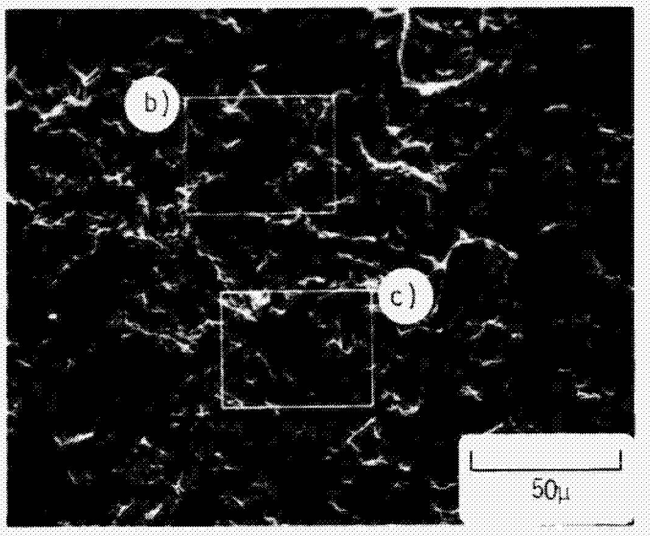

a)

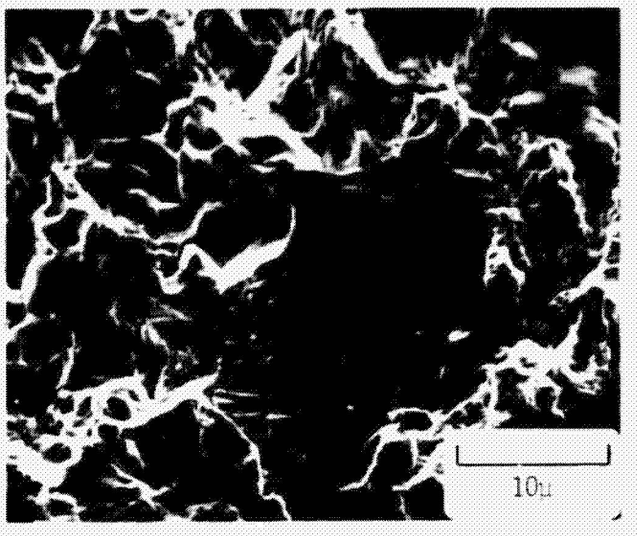

b)

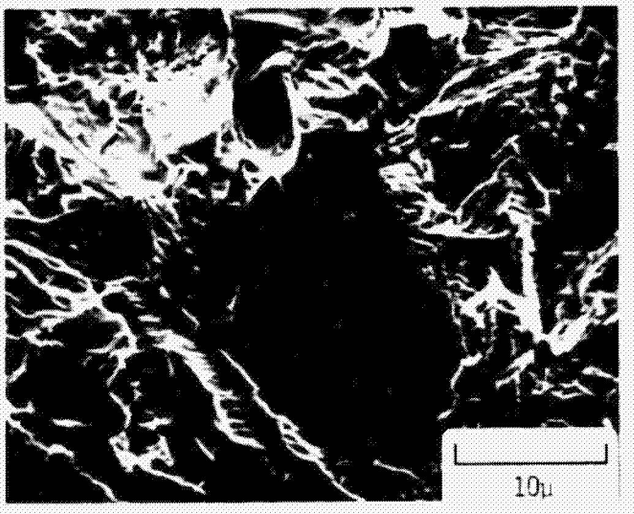

c)

Figure 26 - X-60 Fatigue Surface of the Base Metal Produced in 6.9 MPa H_2. a) General View of Failure; b) High Magnification Fractograph of a Cleavage Area; c) High Magnification Fractograph of a Transgranular Cyclic Cleavage Area.

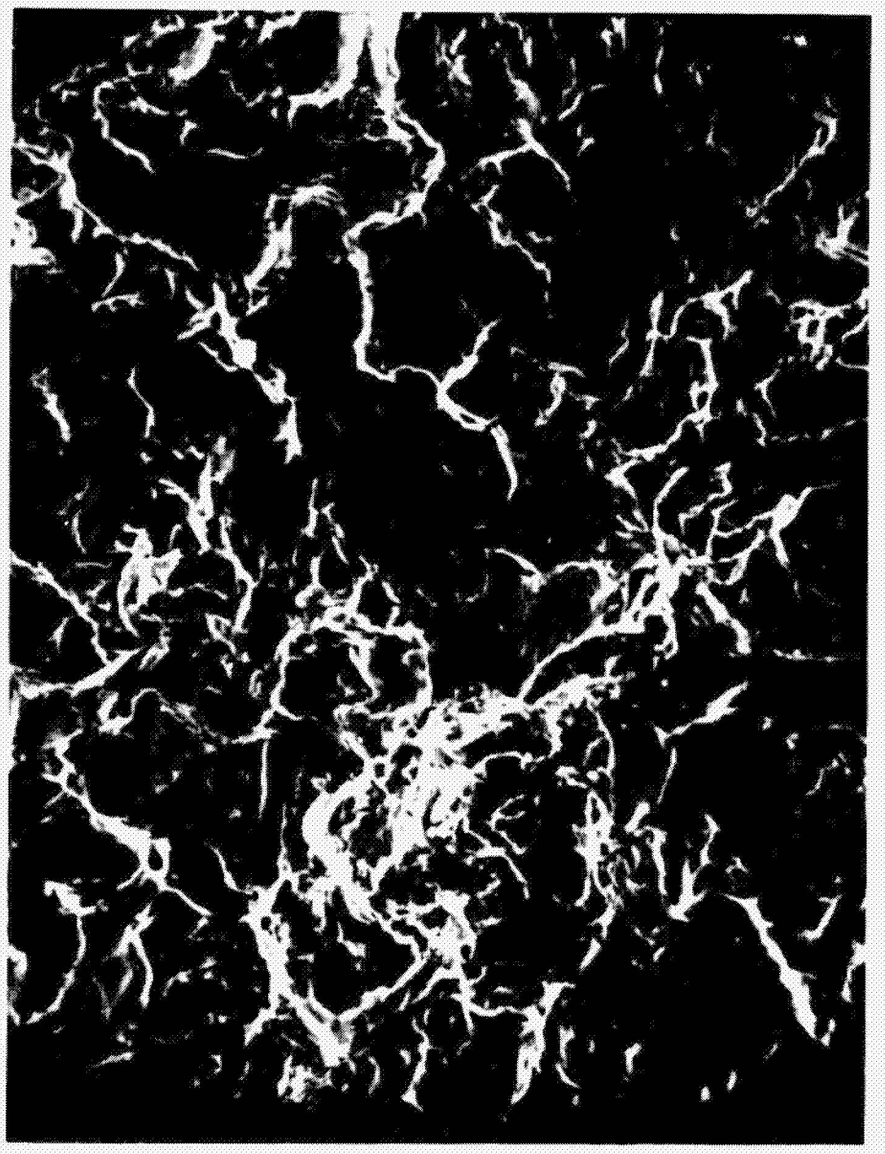

Figure 27 - Failure Surface of X-60 Base Metal Exhibiting Substantial Intergranular Secondary Cracking.

As ΔK decreases and the crack growth rate approaches 10^{-9} m cycle^{-1}, the influence of the A516 microstructure becomes more pronounced. The air threshold value of 9 MPa$\cdot m^{1/2}$ for the 900°C normalized microstructure is in good agreement with the results of Aita and Weertman[24] and Masounave and Bailon[25] who used a variety of pearlitic-ferritic steels. At present there are no threshold values for comparable quenched and tempered martensitic or bainitic microstructures or for a variety of prior austenitic grain sizes. However, Minakawa and McEvily[26] recently reported a fatigue threshold value of $\Delta K_0 \simeq 14$ MPa$\cdot m^{1/2}$ for a duplex ferritic-martensitic steel. This is in good agreement with the threshold values obtained for the A516 martensitic and bainitic microstructures that were austenitized at 1200°C.

The fatigue crack growth behavior of both A516 and X-60 steels is greatly influenced by the presence of a high pressure hydrogen environment. The FCGR is increased by as much as a factor of ten above that observed in air; compare Figure 7 and 8 or Figure 9 and 10. These results are in good agreement with earlier results of Nelson[2] on a ferritic-pearlitic SAE 1020 steel. The threshold alternating stress intensities for fatigue crack growth are also lower in hydrogen compared to those obtained in air for all the A516 microstructures. No thresholds for the X-60 microstructure were measured during this study. However, Ritchie has measured the fatigue threshold for an X-60 material in 0.1 MPa (1 atm) hydrogen and reported a value of $\Delta K \simeq 8$ MPa$\cdot m^{1/2}$ at 10^{-9} m/cycle[27]. Additionally, he has studied a 2 1/4 Cr - 1 Mo steel[28] and found an alternating stress intensity of 9 MPa$\cdot m^{1/2}$ at 10^{-9} m/cycle. Both of these materials had been austenitized in the 900°C range. These results of Ritchie are in good agreement with the threshold for the 900°C normalized A516 microstructure of this study.

The decrease in threshold observed in hydrogen was more severe in the A516 ferritic-pearlitic microstructures (12% decrease) than in the martensitic microstructures (6% decrease). The fact that martensitic microstructures exhibit higher thresholds and therefore have a higher resistance to early crack growth may be a partial explanation for the observed fact that in high strength steels, the best resistance to hydrogen in an aqueous environment is found in the well tempered martensitic and bainitic microstructures[17,18]. However, comparison of these results may not be valid, because the mechanisms of hydrogen degradation in the high strength steels under a static load may not be the same as for this low strength steel under dynamic loads. Further experimentation is required to fully understand the additional hydrogen resistance observed in these cyclic crack growth tests.

The single most important microstructural variable found in this study is the prior austenitic grain size. The fatigue threshold stress intensity value is increased with increasing austenitic grain size. This has been observed by others and is the general behavior for high strength steels[14], precipitation hardened ferrites[29] and plain carbon steels[25]. Present results indicate the same trend occurs for the hydrogen fatigue threshold as well. In both air and hydrogen, the fatigue threshold is observed to increase a minimum of 25% for a factor of ten increase in austenitic grain size. Finally, these results suggest that in welded structures, material experiencing the lowest austenitizing temperatures, such as in the base plate or at the parent metal - transition zone interface, may be more susceptible to early flaw growth or propagation of flaws at lower stress levels than in similar material which has experienced higher austenitizing temperatures such as in the HAZ and fusion

zone. Unfortunately, the threshold values were not measured for the welded X-60 material. However, a direct measure of the threshold for the transition zone alone would not have been possible due to the mixed microstructures along the crack front.

Another parameter found to influence near threshold fatigue behavior is the strength level. In the present study as the strength level increases for a given austenitizing temperature, the threshold fatigue value also increases. This increase, although small, is found to exist in both air and hydrogen. This shift in threshold is contrary to what has been seen by others in both low-strength[25,28,29] and ultra-high strength steels[14]. However, Minakawa and McEvily[26] have reported an increase in the threshold with increasing strength of duplex ferritic-martensitic microstructures. They suggested that a large crack closure occurs due to back stresses and confinement of plastic deformation associated with the hard martensite. Their analysis indicates that ΔK_{eff} is approximately the same for the variety of duplex ferrous microstructures tested. A similar situation may exist in the present microstructure whereby the quenched and tempered microstructures constrain the amount of plastic deformation that can occur at the crack tip. This constraint is also suggested by fractogrphic evidence of reduced plastic deformation processes on the fracture surface of the quenched and tempered specimens (Figs. 5 and 6). However, no measurements of crack closure or effective ΔK were made in this study to verify their proposal.

CONCLUSIONS

The role of microstructure on the near-threshold fatigue behavior has been determined for two low strength, low alloy steels. The fatigue crack growth rate above an alternating stress intensity of ~ 15 $MPa \cdot m^{1/2}$, whether in air or high pressure hydrogen, was found to be independent of microstructure, strength level, and small variations in steel chemistry.

The fatigue threshold values at $10^{-9} ms^{-1}$ were determined for several normalized, and quenched and tempered microstructures produced in an A516-G70 steel. Both an austenitic grain size dependence and a strength level dependence of the near-threshold fatigue behavior were observed. The fatigue threshold value increased with increased austenitic grain size and increased yield strength. In addition, the threshold values were found to decrease in a hydrogen environment - the martensitic microstructures showing the largest decrease, normalized microstructures showing the least.

From these results, quench and tempered microstructures produced at higher austenizing temperatures appear to provide the best static strength and near-threshold fatigue behavior in both air and high pressure hydrogen environments. The typical hot-rolled, normalized microstructure resulted in the lowest static strength and lowest fatigue threshold value. Any final consideration of an appropriate material should also include the effect of microstructure on fracture toughness. This area was not addressed in this study. In summary, microstructure does influence the near-threshold fatigue behavior in both air and in gaseous hydrogen.

REFERENCES

1. Clark, W. G., Jr., Hydrogen in Metals, A.W.Thompson & I.M.Bernstein, eds., p. 149, TMS-AIME, New York, NY, 1974.

2. Nelson, H.G., Proc. of 2nd Int. Conference on Mechanical Behavior of Materials, pp 690-699, Boston, August 1976.

3. Louthan, M.R., Jr., and McNitt, R.P., Annual Report on "The Roles of Rate and State of Stress Controlling Susceptibility to Hydrogen Embrittlement," VPI & SU, Blacksburg, Va., October 1979.

4. Mucci, J., Final Report on "Evaluation of Laser Welding Techniques for Hydrogen Transmission," Pratt and Whitney Aircraft Group, West Palm Beach, FL, May 1980.

5. Nelson, H.G., "Hydrogen Induced Slow Crack Growth of a Plain Carbon Pipeline Steel under Conditions of Cyclic Loading," Effects of Hydrogen on Behavior of Materials, A.W.Thompson and I.M. Bernstein, eds., AIME New York, NY, pp 602-611, 1976.

6. Hoover, W.R., Iannucci, J.J., Robinson, S.L., Spingarn,J.R., and Stoltz, R.E., Annual Report for DOE - Hydrogen Compatibility of Structural Materials for Energy Storage and Distribution, SAND79-8202, Sandia Laboratory, Livermore, CA, 1980.

7. Ritchie, R.O., "Analytical and Fracture Mechanics," Proceedings of International Conference, G.C.Sijthoff, ed., Sijthoff and Noordhoff, Rome, Italy, 1980.

8. Ritchie, R.O., Suresh, S., Moss, C.M.,"Near-Threshold Fatigue Crack Growth in 2¼ Cr - 1 Mo Pressure Vessel Steel in Air and H_2",J. of Eng. Materials and Technology, Vol. 102, pp 293-299, July 1980.

9. Ritchie, R.O., and Knott, J.F., Acta Met., 21, p 639, 1973.

10. Beevers, C.J., Cooke, R.J., Knott, J.F. and Ritchie, R.O., Met. Sci., 9, p 119, 1975.

11. Ritchie, R.O., International Metals Reviews, 20, p 205, 1979.

12. Ritchie, R.O., Met. Trans., 8A, p 1131, 1977.

13. Benson, J.P. and Edmonds, D.V., Metal Science, 12, p 223, 1978.

14. Ritchie, R.O., Metal Science, 11, p 368, 1977.

15. Bernstein, I.M., and Thompson, A.W., International Metals Reviews, 21, p 267, 1976.

16. Chandler, W.T., and Walter, R.J., Hydrogen Energy, T.N. Vezitoglu, ed., p 1057, Penum Press, New York, NY, 1975.

17. Hobson, J.D., and Sykes, C., JISI, 169, p 209, 1951.

18. Snape, E. Corrosion, 24, p 251, 1968.

19. Newman, J.C., Jr., ASTM STP560, p 105, ASTM, Philadelphia, PA, 1974.

20. Banerjee, S., Private Communication.

21. Spingarn, J., Private Communication.

22. Sullivan, A.M., and Crooker, T.W., NRL Report No. 8004, Naval Research Laboratory, Washington, D.C., 1974.

23. Wilson, A.D., J. Eng. Mat & Tech., 101, p 265, 1979.

24. Aita, C.R., and Weertman, J., Met Trans., 10A, p 535, 1979.

25. Masounave, J., and Bailon, J.B., Scripta Met., 10, p 165, 1976.

26. Minakawa, K., and McEvily, A.J., Proc. 5th Int. Conf. on Strength of Metals and Alloys, P. Haasen, ed., Pergamon Press, New York, NY, 1979.

27. Ritchie, R.O., Private Communication, 1980.

28. Ritchie, R.O., MIT Fatigue and Plasticity Lab Report No. FPL /R/80/1032, MIT, Boston, MA, April 1980.

29. Benson, J.P., Metal Science, 11, p 535, 1979.

30. Mitchell, M., Private Communication, 1980.